Role of substituted atoms in stacking fault formation in long-period stacking ordered system

doi: https://doi.org/10.1016/j.commatsci.2019.109210

Role of substituted atoms in stacking fault formation in long-period stacking ordered system

S. Kawano, and S. Iikubo*

Graduate School of Life Science and Systems Engineering, Kyushu Institute of Technology, Kitakyushu 808-0196, Japan

H. Ohtani

Institute of Multidisciplinary Research for Advanced Materials, Tohoku University, 2-1-1 Katahira, Aoba-ku, Sendai 980-8577, Japan

Abstract

To study the formation mechanism of the long-period stacking ordered (LPSO) structures, the reaction pathways of solid–solid transformations from a hexagonal close-packed (HCP) structure to LPSO structures in Mg-Y-Zn alloys were calculated using the generalized solid-state nudged elastic band method. The energy increases along the transition from HCP to 18R, and the peak positions represent the activation energy for the transition. Y substitution hardly changes the activation energy but makes the 18R-type LPSO structure more stable than HCP. In contrast, Zn or Y+Zn substitution results in higher activation energy and makes the 18R-type LPSO structure less stable than HCP. The calculated results for 14H and 24R LPSO structures also show similar activation energy and LPSO stability to the HCP-18R transition. Therefore, Y substitution plays an important role in stabilizing the stacking faults in LPSO systems. For the microscopic mechanism, the volume dependence of the total energy in pure FCC and HCP Y were examined, and the result suggests that FCC-Y is stable than HCP-Y under pressure. Therefore, the effect of substitution of Y in HCP Mg can be explained by the characteristics of Y under the chemical pressure exerted by the small size of Mg lattice.

Keywords: LPSO structure, First-principles calculation, stacking fault

*Corresponding author
S. Iikubo; iikubo@life.kyutech.ac.jp

I. INTRODUCTION

Mg-based alloys are expected to be utilized in the automotive, aviation, aerospace, and electronic industries because of their light weight and natural abundance. To date, the mechanical properties of Mg-based alloys have been improved by adding elements to impart anticorrosion properties, grain refinement strengthening, precipitation strengthening, and so on. Despite these efforts to strengthen them, Mg-based alloys still have much less strength than Al-based alloys; therefore, it is important to increase their strength to enable their widespread use. Among the different types of Mg alloys, those with long-period stacking ordered (LPSO) structures have received attention because of their good mechanical properties, with reported yield strength of above 600 MPa and elongation of 5% at room temperature [1].

LPSO structures are known to be formed in Mg alloys with transition metal and rare earth elements; the typical and most studied one is the Mg-Y-Zn system [1–6]. The LPSO structures can be described as having stacking faults that are introduced periodically into the hexagonal close-packed (HCP) structure, as Y and Zn atoms concentrate on stacking fault layers with a local face-centered cubic (FCC) lattice [2–4], as shown in Fig. 1. These HCP and local FCC lattice structures can coexist because a partial FCC lattice is formed by the glide of the basal plane of the HCP structure with Shockley partial dislocation. The LPSO structures are classified according to their different stacking fault sequences and whether they exhibit hexagonal (H) or rhombohedral (R) symmetry, for example, 18R, 14H, 24R, and 10H types. Note that, in Figs. 1, 2 and 3, the basal plane shape is based on hexagonal primitive cell. The direction perpendicular to the basal plane indicate [0001] of HCP. The *c*-axis of 18R structure is tilted because of the rhombohedral symmetry.

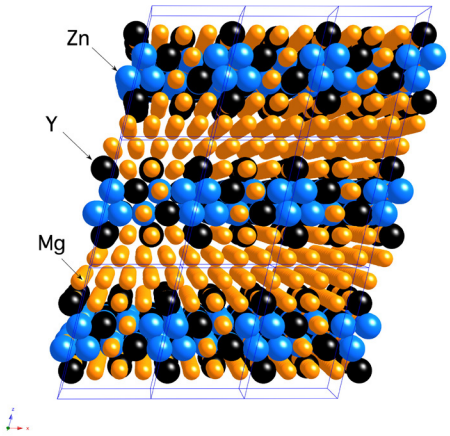

Fig. 1 18R-type LPSO structure [4].

The LPSO formation mechanism has not been comprehensively studied. The $L1_2$-type short-range order observed in the transmission electron microscope experiment [4,7–9] seems to have an important role in the LPSO formation, which is an attractive scenario. Its derivative clusters containing an interstitial atom at their center were proposed [10], and the inter cluster interaction was investigated [11] by conducting a density functional theory (DFT) analysis. The LPSO formation from the amorphous state was investigated using small angle scattering techniques [12], which indicated that randomly placed clusters gradually ordered to form LPSO structure. However, it is controversial whether this behavior is a general formation mechanism for LPSO structures because such cluster ordering, which is a collective motion of atoms, seems to be unfavorable from the energetic point of view.

On the other hand, it is a plausible idea to understand the LPSO formation mechanism as a process of forming a metallographic structure. A hypothesis that considers the LPSO structure for two phases consisting of HCP phase and FCC phase explains its several characteristics. For example, the Mg-Y-Zn ternary system has interesting thermodynamic properties that result in compositional modulation between Mg-rich region and Y-Zn-rich region in the HCP phase [13]. Furthermore, when the system contains stacking faults, Y and Zn concentrate on the stacking fault layer due to the difference in chemical potential between the HCP structure and stacking fault local FCC structure [14]. These calculations reveal the driving force for the segregation of the introduced atoms into the stacking fault. Such segregation process of Y and Zn in LPSO structure was observed by a recent *in situ* XRD measurement [15].

For the stacking fault formation, our group has also calculated free energy including lattice vibration effects. The stabilization of 14H- and 18R-types long periodic structures were clearly revealed in “pure Mg” at finite temperature; however, the energy gain was quite small (~ meV) [16]. According to these previous studies, the formation of stacking faults with substituted atoms seems to have an important role in the transition between HCP and LPSO structures. Therefore, we calculated energy variation by means of first-principles calculation of the transition states between HCP and LPSO structures to investigate the effect of substituted atoms on the formation of stacking faults in LPSO systems.

.

II. CALCULATION PROCEDURE

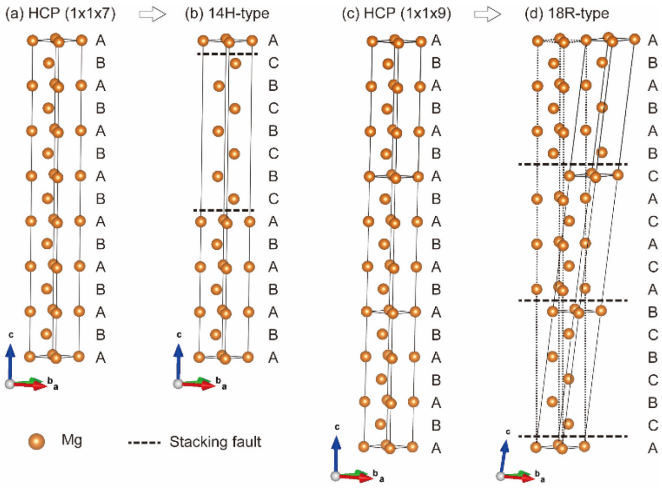

Fig. 2 Model of structural transitions of 14H- and 18R-LPSO structures from an initial HCP structure.

Figure 2 shows the model of the structural transitions of 14H- and 18R-LPSO structures from an initial HCP structure. In the case of 14H, the initial structure is an HCP 1 × 1 × 7 supercell (stacking sequence is ABABABABABABABA), as shown in Fig. 2(a). By introducing a stacking fault, denoted by a dashed line, into the structure every 7 layers, the 14H structure (ABABABA|CBCBCBC|A) is created, as shown in Fig. 2(b). Similarly, Figs. 2(c) and 2(d) show the model of the structural transition of an 18R-LPSO structure. In this case, the initial structure is an HCP 1 × 1 × 9 supercell (stacking sequence is ABABABABABABABABABA), as shown in Fig. 2(c). By introducing a stacking fault into this structure every 6 layers, the 18R structure (A|CBCBCB|ACACAC|BABABA) is created, as shown in Fig. 2(d). In Fig. 2(d), the calculated primitive cell consisting of 6 layers is denoted by a solid line, whereas the conventional cell of the 18R structure is denoted by the dotted line.

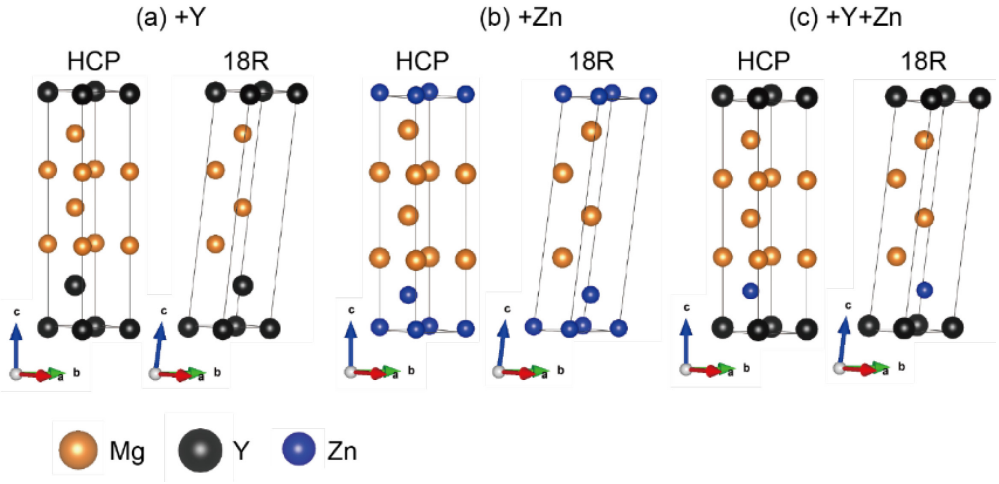

Fig. 3 Crystal structure models of HCP and 18R structures with substituted atoms.

We introduced substituted atoms to the structural model (Fig. 3) near the stacking fault site as two enriched layers. Figure 3 shows the structural models of the HCP and 18R structures used to calculate the effect of substituted elements for (a) Y doping, (b) Zn doping, and (c) Y and Zn co-doping. The same concept was adopted for 14H and other types of LPSO structures. We used these simple models to clearly reveal the effect of substituted atoms. These structure visualizations were performed using the VESTA software [17].

For the calculation of the transition states between HCP and LPSO structures, we employed the generalized solid-state nudged elastic band (SSNEB) method implemented in the Transition State Tools for VASP (VTST) code [18]. Within the SSNEB method, the atomic and cell degrees of freedom are simultaneously relaxed during the calculation. Therefore, it is possible to determine the transition states in solid–solid transformations with different unit cells. We performed structure optimization for the initial and final states, where the HCP structure represented the initial state and LPSO structures represented the final states. Next, we determined the transition state from the initial transition state using a linear interpolation of cell vectors and atomic positions between the initial and final states. To compute the force and energy of these states, we performed first-principles calculations based on the density functional theory (DFT) using the Vienna ab initio simulation package (VASP) [19,20]. The interaction between the ion core and valence electrons was described using the projector-augmented wave method [21,22]. The exchange and correlation functions were given by the generalized gradient approximation, as proposed by Perdew et al. [23,24]. We set the plane wave energy cutoff to 500 eV. The Brillouin zone sampling was performed in a primitive cell using a Γ-point-centered k-mesh that was limited to 0.15 $Å^{-1}$; for example, a 15 × 15 × 8 mesh containing two magnesium atoms was used for the HCP structure. The convergence criterion for electronic self-consistency and ionic relaxation loop

were set to 1×10^{-5} eV and 5×10^{-3} eV, respectively. For the HCP-18R transition with Y+Zn co-doping, the convergence criterion for ionic relaxation was set to 2×10^{-2} eV because of its difficulty of convergence. We used the Methfessel-Paxton smearing method with the smearing width of 0.2 eV. The calculated structures were fully optimized with respect to the volume and shape of the unit cell and atomic positions.

III. RESULTS

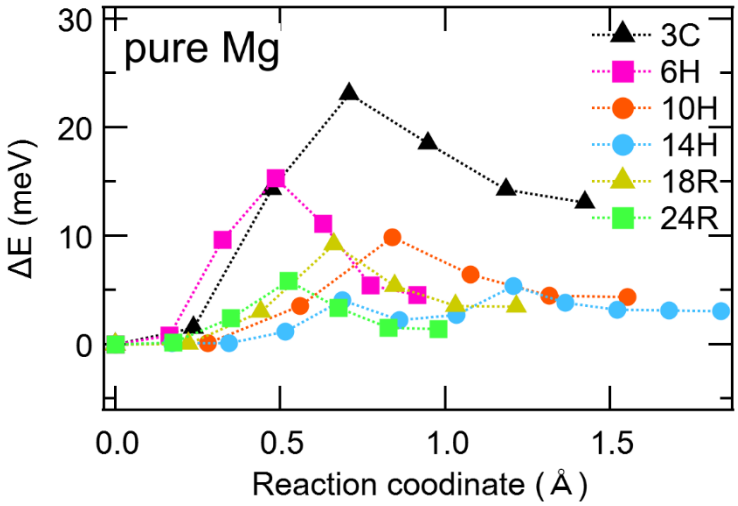

Fig. 4 Energy transition of pure Mg during transformation from HCP to different types of LPS structures.

Figure 4 shows the energy transition for the transformation from HCP to LPS structures. Note that these calculations were performed for pure Mg. The energy transition ΔE is calculated as follows:

$$\Delta E = E_{\text{image}} - E_{\text{HCP}} \quad (1)$$

, where E_{image} is the total energy per atom of each image during transition and E_{HCP} is the total energy per atom of HCP. On the SSNEB method, the reaction coordinate is defined by cell vector and atomic position change. However, these variables have different unit. To combine these variables, a Jacobian J which has the unit of length is employed [18]. Therefore, the reaction coordinate which is the norm of the strain and the atomic position change is defined as follows:

$$\|\Delta \boldsymbol{R}\| = \sqrt{J^2\|\boldsymbol{\varepsilon}\|^2 + \|\Delta \boldsymbol{r}\|^2}, \quad (2)$$

where $\boldsymbol{\varepsilon}$ is the strain for describing cell vector change and $\Delta \boldsymbol{r}$ is the atomic position change. This is the reaction coordinate for each model which is shown as the horizontal axis in the figure. J is defined as follows:

$$J = \sqrt{N}L, \; L = \left(\frac{V}{N}\right)^{1/3}, \quad (3)$$

where N is number of atoms in the unit cell, V is the volume of the cell, and L is the average distance between atoms in the cell.

In Fig. 4, HCP is the most stable state of all the calculated phases; this is well known as the stable phase. ΔE_{stable}, which indicates the stability of the final state, is 13 meV for FCC. This value is well consistent with the values cited in the Materials Project [25] and the Open Quantum Materials

Database [26,27], which are 11 meV and 13 meV, respectively. The energy difference ΔE_{stable} between the HCP and LPS structures is less than 5 meV, except between HCP and FCC. The activation energy ΔE_a is relatively large for FCC and 6H, which are relatively short period stacking ordered structures, and low for other LPSO structures (< 10 meV). ΔE_{stable} decreases as the period of stacking faults increases. This tendency seems to be plausible because the increasing period of stacking faults means that the structure with stacking faults finally reaches HCP stacking, which is the reference state.

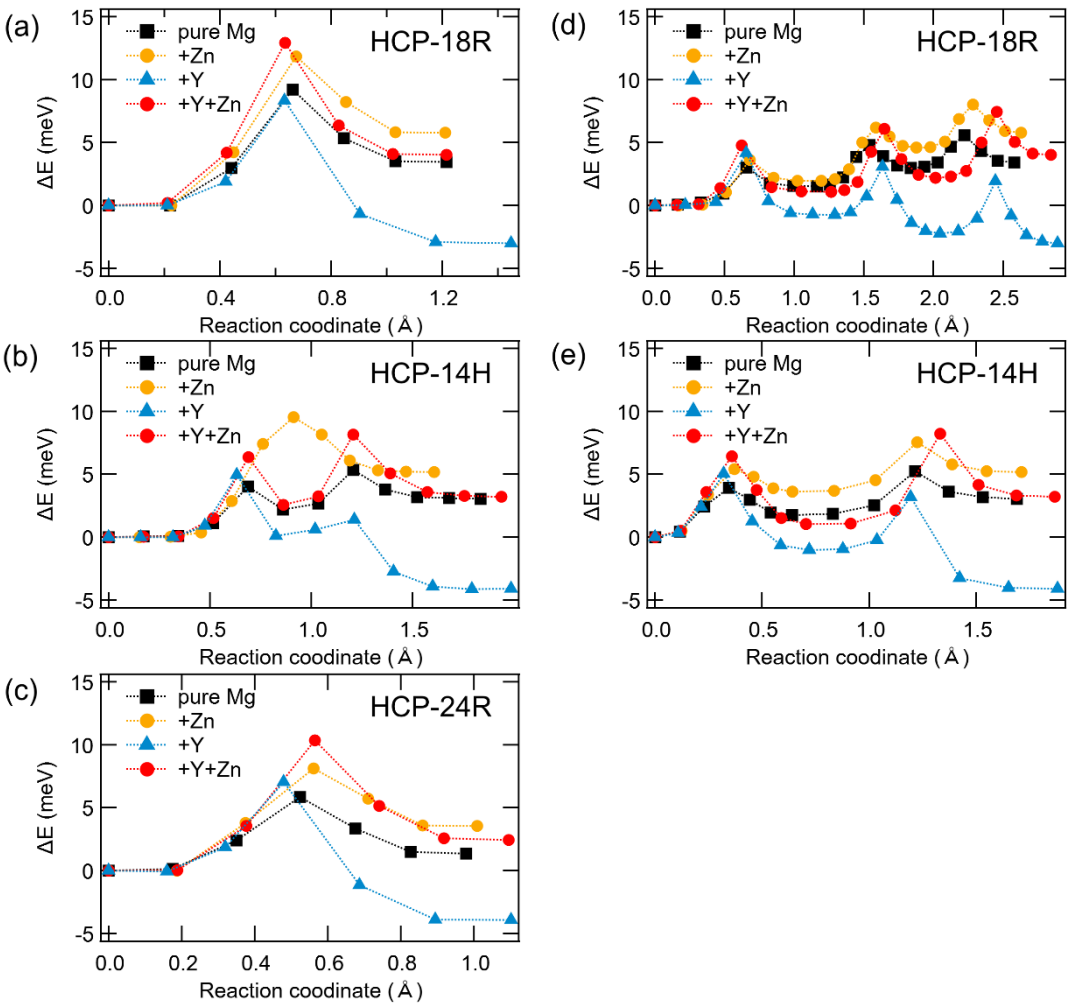

Fig. 5 Energy transition of pure Mg and Mg with Zn and/or Y doping during the transformation from HCP to different types of LPSO structures.

We considered the effect of Zn and/or Y on the transformation from HCP to 18R, 14H, and 24R structures. Figs. 5 (a)–(c) show the energy transition of pure Mg and Mg with Zn and/or Y during

the transformation from HCP to 18R, 14H, and 24R. The Zn-doped system, denoted by yellow line, shows higher activation energy and lower LPSO stability than pure Mg. The Y and Zn co-doped system, denoted by red line, shows high activation energy and a similar LPSO stability as pure Mg. The Y-doped system, denoted by blue line, shows a similar activation energy as pure Mg, and the LPSO structure is more stable than HCP. These results clearly show that Y has an effect on the stacking fault formation.

In Fig. 5(b), two peak structures can be seen in the middle of the 14H-LPSO transformation. For the transition from HCP to the 14H-LPSO structure, two stacking faults need to be introduced. Unlike our expectation that these stacking faults occur simultaneously, a two-step stacking fault introduction occurred in the 14H unit cell. It should be verified whether the observed chemical effect on the stacking fault formation can be changed, depending on the intermediate state. To clarify the model dependence of this chemical effect, the intermediate states were considered for the 14H and 18R structures. For this purpose, a supercell of dimensions 1 × 1 × 3 was introduced for the HCP-18R transition. Figs. 5(d) and 5(e) show the energy transition of pure Mg and Mg with Zn and/or Y doping during transformation, which apparently consider the intermediate states. We can clearly see peak structures corresponding to the introduction of stacking faults. In the transition from HCP to the 18R-LPSO structure, three stacking faults need to be introduced. These calculations show similar activation energy and LPSO stability to those shown in Figs. 5(a) and 5(b). We observed that ΔE_{stable} clearly decreased with Y; therefore, these results indicate that a stacking fault is likely to be formed at Y-concentrated layer. We considered that such differences in the sequence of stacking faults did not affect our efforts to determine the role of substituted atoms.

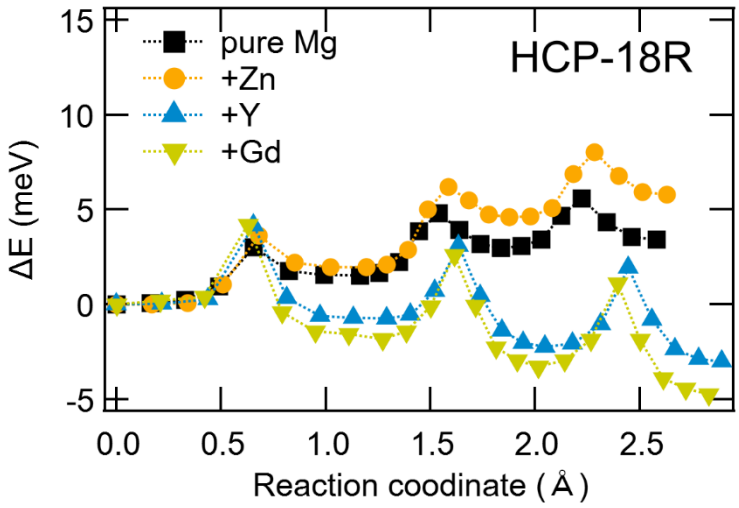

Fig. 6 Effect of Gd on energy transition for transformation compared to results of Zn, Y, and pure Mg.

Another typical LPSO structure is observed in the Mg-Gd-Al ternary system. In this system, the rare earth element is Gd that is expected to play an important role in the stabilization of the stacking fault formation, instead of Y. Figure 6 shows the effect of Gd doping on the energy transition for the HCP-18R transformation compared to results of Zn, Y, and pure Mg. The figure also shows that ΔE_{stable} decreases with Gd; this is the same trend as that observed for Y. Therefore, a Gd layer facilitates the formation of stacking faults.

IV. DISCUSSION

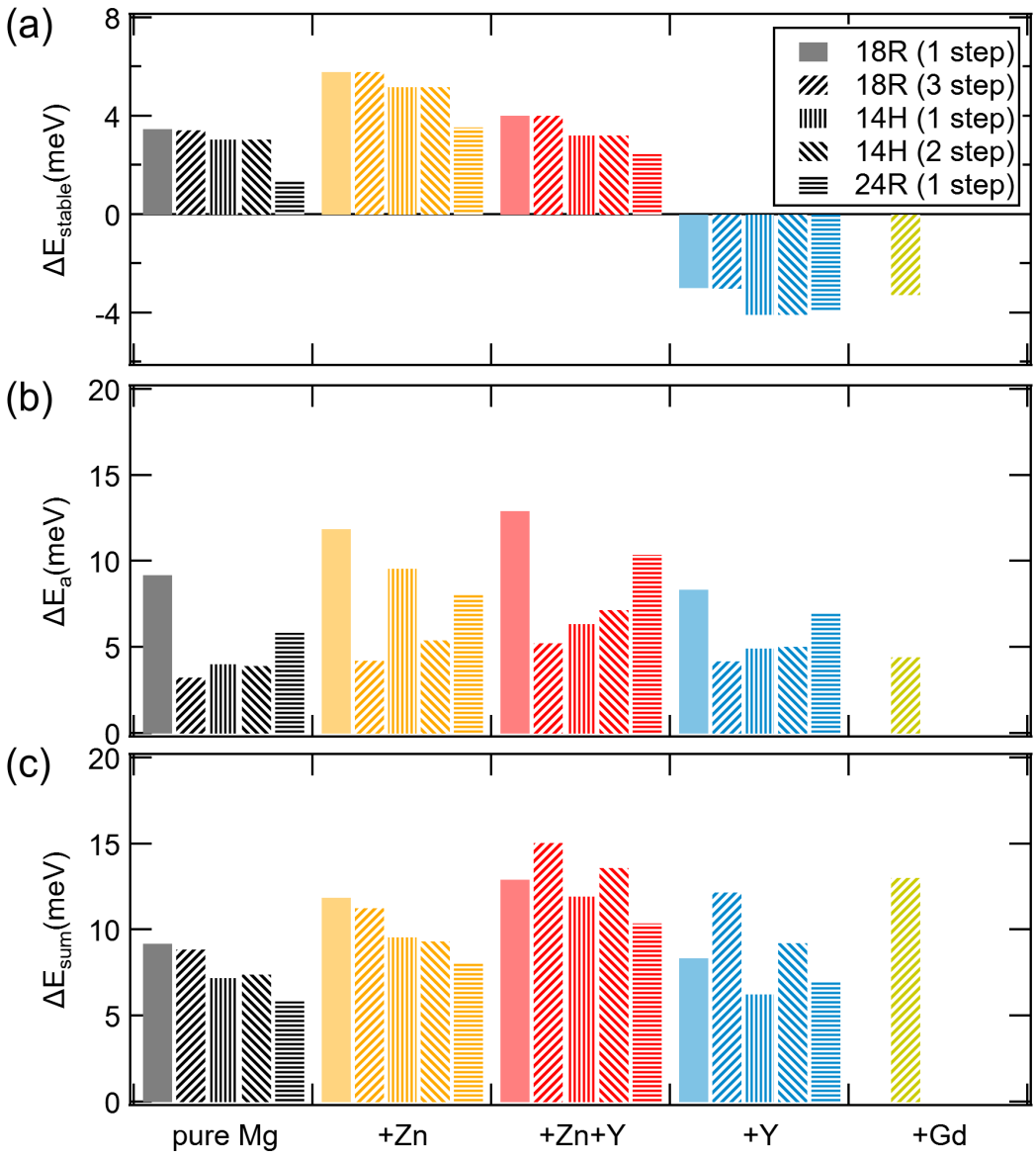

Fig. 7 Summary of LPSO stabilization energy ΔE_{stable} and activation energy ΔE_a and ΔE_{sum} for different doping systems.

Our solid-state nudged elastic band (SSNEB) calculations are summarized in Fig. 7. The results obtained considering the intermediate states are labelled as 3-step and 2-step for 18R and 14H. ΔE_{stable} in Fig. 7 (a) indicate the stability of the final state. To consider the energy of barrier of LPSO formation in multi-step process, we assumed two concept which are "the highest energy in each barrier ΔE_a" or "sum of each barrier energy ΔE_{sum}". ΔE_a and ΔE_{sum} are represented in Fig. 7 (b) and (c), respectively. As compared to pure Mg, in Fig. 7 (a), the Zn-doped system have slightly

high ΔE_{stable} values and Zn and Y co-doped system have similar ΔE_{stable}, whereas the Y-doped system has low ΔE_{stable}. From this analysis, the decreasing ΔE_{stable} by Y-dope is the particularly remarkable effect. In Fig. 7 (b), Zn-doped and co-doped system have slightly high ΔE_a and Y-doped system have similar ΔE_a. In Fig. 7 (c) seems to follow the similar trend to Fig. 7 (b). There is less atomic effect to the activation energy by doped atom in our calculation. The Gd system seems to follow the same trend as the Y system. These results show that Y and Gd have the effect of stabilizing the stacking faults in LPSO systems.

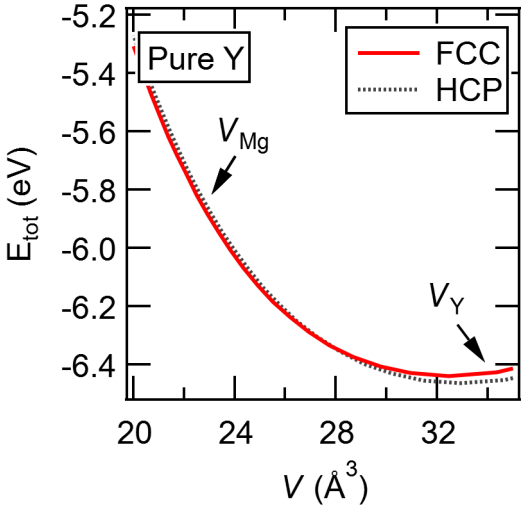

Fig. 8 Calculated volume dependence of total energy of FCC and HCP phases of pure Y.

As a plausible explanation for the role of Y in the stacking fault formation, we would like to propose that chemical pressure must act on Y in the HCP-Mg. Both pure Y and Mg have an HCP lattice as a ground state, but their lattice constants are different with a = 3.6474(7) and c = 5.7306(8) for Y, and a = 3.2125(5) and c = 5.2132(8) for Mg [28,29]. Therefore, doped Y atoms should feel a positive chemical pressure from the HCP-Mg lattice.

We estimated the effect of the chemical pressure of Y-concentrated LPSO. However, complex and difficult calculation is necessary to estimate the chemical pressure dependence of the LPSO stability. Because we need to apply the pressure in a part of LPSO structure which is Y-concentrated layer. Therefore, we simply assumed that the chemical pressure dependence of the LPSO stability can be approximated by the energy-volume diagram of HCP and FCC phases of pure Y. To estimate the effect of chemical pressure based on above assumption, the volume dependence of total energy in both FCC and HCP structures of pure Y are calculated under external pressure ranging from $P = -8$ GPa to 50 GPa in steps of 2 GPa. Figure 8 shows the calculated volume dependence of the total energy of the FCC and HCP phases of pure Y. V_{Mg} and V_Y are experimental volumes of the HCP phase of each element. Although the stable state is the

HCP phase at V_Y, the stable state changes to the FCC phase at V_{Mg}. This is a reasonable result for the above chemical pressure scenario. There is a related experimental result that the crystal structure sequence HCP → Sm type → double HCP → mixed (double HCP + FCC) → distorted FCC is observed below 50 GPa [30]. These structures are considered to be formed by the introduction of stacking faults into the HCP structure under an external pressure. For the LPSO formation, Y under chemical pressure in the HCP-Mg lattice is likely to be an FCC structure and act as a trigger for the stacking fault formation, which is locally an FCC structure. We considered Gd to have a role in forming stacking faults by chemical pressure because Gd is reported to have a similar crystal structure sequence as Y under pressure [31]. Therefore, these rare-earth elements may have a role in forming stacking faults. In fact, Y can be substituted by Gd, Tb, Dy, Ho, Er, or Tm [32]. This conclusion suggests that elemental properties are one of the factors that make a good substitute for Y.

On the other hand, the role of Zn in the increase of ΔE_a and ΔE_{stable} is not clear from the current results. Zn has an unusually large c/a ratio of 1.857 at 300 K [33] (ideal value c/a ratio: ~ 1.633, Mg HCP: ~ 1.623). The lattice mismatch between Mg and Zn in the HCP structure is large. We speculate that ΔE_a and ΔE_{stable} are affected by the lattice mismatch. A previous study showed that Zn and rare-earth atoms segregate to the stacking fault, mainly because of the difference between the chemical potentials of each element of the FCC and HCP structures [34]. This is called the Suzuki effect [35]. Therefore, Zn contributes to such segregation rather than the formation of stacking faults.

V. CONCLUSION

We reported the role of substituted atoms in the formation of stacking faults, which is a part of the formation mechanism of LPSO structures, by using first principles calculations along with the generalized solid-state nudged elastic band method. The energy profile for the HCP-LPSO transition clearly shows that a Y-concentrated layer in the HCP structure can easily form a stacking fault. Furthermore, we concluded that the role of substituted Y is caused by the properties of pure Y resulting from a chemical pressure. The results provide important information about the formation of stacking faults, which is the central topic of the LPSO formation mechanism. We suggest that the substituted atoms that are affected by chemical pressure are important for the formation of stacking faults for LPSO formation.

ACKNOWLEDGMENTS

We are grateful to Prof. M. Matsushita for helpful discussions about the experiments. This work was supported by the MEXT KAKENHI Grant Number 23109005. This work was also performed under the Cooperative Research Program of "Network Joint Research Center for Materials and Devices".

Reference

[1] Y. Kawamura, K. Hayashi, A. Inoue, and T. Masumoto, Mater. Trans. **42**, 1172 (2001).

[2] J.-K. Kim, W.-S. Ko, S. Sandlöbes, M. Heidelmann, B. Grabowski, and D. Raabe, Acta Mater. **112**, 171 (2016).

[3] Y. M. Zhu, M. Weyland, A. J. Morton, K. Oh-ishi, K. Hono, and J. F. Nie, Scripta Mater. **60**, 980 (2009).

[4] D. Egusa and E. Abe, Acta Mater. **60**, 166 (2012).

[5] M. Matsuda, S. Ii, Y. Kawamura, Y. Ikuhara, and M. Nishida, Materials Science and Engineering: A **393**, 269 (2005).

[6] T. Itoi, T. Seimiya, Y. Kawamura, and M. Hirohashi, Scripta Mater. **51**, 107 (2004).

[7] H. Yokobayashi, K. Kishida, H. Inui, M. Yamasaki, and Y. Kawamura, Acta Mater. **59**, 7287 (2011).

[8] K. Kishida, H. Yokobayashi, H. Inui, M. Yamasaki, and Y. Kawamura, Intermetallics **31**, 55 (2012).

[9] K. Kishida, H. Yokobayashi, and H. Inui, Philos. Mag. **93**, 2826 (2013).

[10] S.-Y. Ma, L.-M. Liu, and S.-Q. Wang, Journal of Materials Science **48**, 1407 (2012).

[11] H. Kimizuka, M. Fronzi, and S. Ogata, Scripta Mater. **69**, 594 (2013).

[12] H. Okuda, T. Horiuchi, T. Tsukamoto, S. Ochiai, M. Yamasaki, and Y. Kawamura, Scripta Mater. **68**, 575 (2013).

[13] R. Masumoto, H. Ohtani, and M. Hasebe, J. Japan Inst. Met. Mater. **73**, 683 (2009).

[14] S. Iikubo, T. Umebayashi, and H. Ohtani, Proceedings of PRICM8 **2**, 1183 (2013).

[15] M. Matsushita *et al.*, Mater. Trans. **60**, 237 (2019).

[16] S. Iikubo, K. Matsuda, and H. Ohtani, Phys. Rev. B **86**, 054105 (2012).

[17] K. Momma and F. Izumi, J. Appl. Crystallogr. **44**, 1272 (2011).

[18] D. Sheppard, P. Xiao, W. Chemelewski, D. D. Johnson, and G. Henkelman, J. Chem. Phys. **136**, 074103 (2012).

[19] G. Kresse and J. Furthmüller, Comp. Mater. Sci. **6**, 15 (1996).

[20] G. Kresse and J. Furthmuller, Phys. Rev. B **54**, 11169 (1996).

[21] P. E. Blöchl, Phys. Rev. B **50**, 17953 (1994).

[22] G. Kresse and D. Joubert, Phys. Rev. B **59**, 1758 (1999).

[23] J. P. Perdew, K. Burke, and M. Ernzerhof, Phys. Rev. Lett. **77**, 3865 (1996).

[24] J. P. Perdew, K. Burke, and M. Ernzerhof, Phys. Rev. Lett. **78**, 1396 (1997).

[25] A. Jain *et al.*, APL Materials **1**, 011002 (2013).

[26] J. E. Saal, S. Kirklin, M. Aykol, B. Meredig, and C. Wolverton, JOM **65**, 1501 (2013).

[27] S. Kirklin, J. E. Saal, B. Meredig, A. Thompson, J. W. Doak, M. Aykol, S. Rühl, and C. Wolverton, npj Computational Materials **1** (2015).

[28] P. Karen, A. Kjekshus, Q. Huang, and V. L. Karen, J. Alloys Compd. **282**, 72 (1999).

[29] F. H. Spedding, A. H. Daane, and K. W. Herrmann, Acta Crystallogr. **9**, 559 (1956).

[30] G. K. Samudrala, G. M. Tsoi, and Y. K. Vohra, J. Phys. Condens. Matter. **24**, 362201 (2012).

[31] D. Errandonea, R. Boehler, B. Schwager, and M. Mezouar, Phys. Rev. B **75** (2007).

[32] Y. Kawamura and M. Yamasaki, Mater. Trans. **48**, 2986 (2007).

[33] J. Nuss, U. Wedig, A. Kirfel, and M. Jansen, Z. Anorg. Allg. Chem. **636**, 309 (2010).

[34] T. Umebayashi, S. Iikubo, and H. Ohtani, J. Japan Inst. Met. Mater. **78**, 117 (2014).

[35] H. Suzuki, Sci. Rep. Res. Inst. Tohoku Univ. A **4**, 455 (1952).